

# Elucidating image-to-set prediction: An analysis of models, losses and datasets

Luis Pineda<sup>1\*</sup>, Amaia Salvador<sup>2\*†</sup>, Michal Drozdal<sup>1</sup>, Adriana Romero<sup>1</sup>

<sup>1</sup>Facebook AI Research <sup>2</sup>Universitat Politecnica de Catalunya

amaia.salvador@upc.edu, {lep, mdrozdal, adrianars}@fb.com

## Abstract

*In this paper, we identify an important reproducibility challenge in the image-to-set prediction literature that impedes proper comparisons among published methods, namely, researchers use different evaluation protocols to assess their contributions. To alleviate this issue, we introduce an image-to-set prediction benchmark suite built on top of five public datasets of increasing task complexity that are suitable for multi-label classification (VOC, COCO, NUS-WIDE, ADE20k and Recipe1M). Using the benchmark, we provide an in-depth analysis where we study the key components of current models, namely the choice of the image representation backbone as well as the set predictor design. Our results show that (1) exploiting better image representation backbones leads to higher performance boosts than enhancing set predictors, and (2) modeling both the label co-occurrences and ordering has a slight positive impact in terms of performance, whereas explicit cardinality prediction only helps when training on complex datasets, such as Recipe1M. To facilitate future image-to-set prediction research, we make the code, best models and dataset splits publicly available at: <https://github.com/facebookresearch/image-to-set>.*

## 1. Introduction

Major advances in image understanding tasks [57, 18, 50, 49, 37, 23, 17] have been enabled by the introduction of large scale datasets such as ImageNet [53], MSCOCO [30] or Cityscapes [10]. All of these datasets come with benchmark suites that target well defined problems, provide dataset splits, and automated evaluation servers to rank methods according to their test set results, thus ensuring a fair comparison among methods. However, building large scale datasets with benchmark suites requires signif-

icant effort, which may not scale well with the increasing number of image understanding tasks and modalities. As a result, researchers often resort to reusing publicly available datasets, without defining rigorous benchmark suites for the task at hand. This lack of rigour leads to contributions with apparent new state-of-the-art results, which are evaluated under different dataset splits, evaluation metrics, experimental budgets [43], and other uncontrolled sources of variations [43, 3]. As such, these seemingly successful empirical outcomes result in unquantifiable progress, raising reproducibility issues and driving potentially inaccurate claims. In the quest to draw sound and robust conclusions, we join other recent papers in highlighting the under-acknowledged existence of conclusion replication failure [47, 36, 39, 26, 19].

In particular, we build a case study for an important computer vision problem, the image-to-set prediction task (also referred to as multi-label classification), as everyday life pictures are typically complex scenes which can be described with multiple concepts/objects. The most widely used large scale dataset to assess the progress of image-to-set prediction is the MS COCO [30] object detection dataset. Table 1 summarizes recent contributions in the image-to-set prediction literature, emphasizing their factors of variation, and displaying their reported results. As shown in the table, the discordance across published methods is surprisingly high, hindering the robustness of method comparison. First, we notice factors of variation that arise from the lack of a well established benchmark suite: (1) different methods use different train, validation and test splits, (2) not all approaches finetune the image representation backbone and (3) some approaches artificially limit the cardinality of the predicted sets. Notably, when validation set information is unavailable (n/a), it is unclear how model selection is performed. However, in cases where code is made publicly available, one can notice that the test set is used either for hyperparameter selection or for model early stopping. Second, we highlight additional factors of variations due

\*Equal contribution.

†Work partially done during internship at Facebook AI Research.

Set predictor	Backbone	Finetuned	Train	Validation	Test	Baseline O-F1	O-F1
Li et al. 2017 [29]	VGG	✓	77977	4104	40137	n/a	62.9*
Wang et al. 2017 [62]	VGG	✓	82081	n/a	40137	n/a	72.0*
Zhang et al. 2018 [71]	VGG	✓	82081	n/a	40137	n/a	66.5*
Chen et al. 2018 [7]	VGG	n/a	82081	n/a	40137	n/a	71.1
Liu et al. 2018 [35]	VGG	✓	82081	n/a	40137	n/a	74.0
Wang et al. 2016 [61]	VGG	✗	82783	n/a	40504	63.3*	67.8*
Rezatofghi et al. 2017 [51]	VGG	✓	74505	8278	40504	62.9*	69.4
Liu et al. 2017 [32]	VGG	✓	82783	n/a	40504	63.3	75.16
Li et al. 2018 [28]	VGG	✓	82783	n/a	40504	59.3	65.2
Rezatofghi et al. 2018 [52]	VGG	✓	74505	8278	40504	69.2*	70.7
Luo et al. 2019 [40]	ResNet-50	✓	n/a	n/a	n/a	63.2	65.2
Ge et al. 2018 [14]	ResNet-101	✓	82081	n/a	40504	76.3	78.4
Zhu et al. 2017 [75]	ResNet-101	✓	82783	n/a	40504	74.4	75.8
Guo et al. 2019 [16]	ResNet-101	✓	82783	n/a	40504	73.7	76.3
Liu et al. 2019 [33]	ResNet-101	n/a	82787	n/a	40504	77.1	79.5
Chen et al. 2019 [8]	ResNet-101	n/a	82081	n/a	40504	76.8	80.3
Chen et al. 2018 [6]	ResNet-152	✗	82783	n/a	40504	61.0	67.7

Table 1: **Overview of image-to-set prediction methods applied to MS-COCO.** Backbone refers to the pre-trained image representation model, whether finetuned or not (n/a indicates the lack of finetuning information). Train, validation and test indicate the number of images used in each split. When validation is n/a, the same split has been used for both validation and test. Baseline O-F1 corresponds to the (reported) results of training each method’s backbone with binary cross-entropy. O-F1 corresponds to each method’s best reported result. Note that \* refers to results which limit the cardinality of predictions to 3 or 4 elements.

to advancements in image classification, namely the choice of image representation backbone. Finally, we draw the reader’s attention to the results reported for a simple baseline model trained with binary cross-entropy which exhibits surprisingly high variance (e.g. for ResNet-101, the best reported baseline score is 77.1%, while the worst reported value for the same model is 73.7%). All these discrepancies raise the question of fair comparison across models, hampering the conclusions about the role of individual model components in image-to-set prediction advancement.<sup>1</sup>

Therefore, in this paper, we argue that enabling the community with a proper benchmark suite is of crucial importance to take firm steps towards advancing image-to-set prediction methods. The proposed benchmark suite is comprised of a unified code-base, including dataset splits for 5 datasets of increasing complexity (Pascal VOC 2007 [13], MS COCO 2014 [30], ADE20k [74], NUS-WIDE [9] and Recipe1M [55]) and a common evaluation protocol designed to assess the impact of architecture innovations, ensure reproducibility of results and, perhaps more importantly, strengthen the robustness of conclusions. Together with the benchmark suite, we provide an extensive study to weigh the influence of prominent innovations and baselines in the image-to-set literature. Moreover, to ensure that dif-

<sup>1</sup>Similar observations can be made for other datasets, e.g. in case of NUS-WIDE dataset, the number of images used by different works varies since the images are downloaded at different times and some download links are inactive [32]. Moreover, even when ensuring the same number of images, the dataset splits are defined randomly [29, 32, 75].

ferences in model performance can be attributed to modeling choices, rather than unbalanced hyperparameter search, we use a fixed budget of tested configurations (allowing all models to have equal opportunity to reach their best results) by means of the HYPERBAND algorithm [27]. Our analysis aims to investigate the importance of key image-to-set prediction model components: the image representation backbone and the set predictor. On the one hand, we are interested in understanding whether architectural improvements from the single-class image classification literature translate into the multi-label classification scenario. On the other hand, we aim to analyze the importance of (1) explicitly modeling label co-occurrences, (2) leveraging label ordering, and (3) including cardinality prediction in the set predictor. Our main observations can be summarized as:

- Image-to-set prediction benefits from architectural improvements in the single label classification literature.
- Explicitly leveraging label co-occurrences and label ordering tends to have a slight positive impact in terms of performance, whereas incorporating cardinality prediction only helps when training on complex datasets, such as Recipe1M.
- Exploiting better image representation backbones tends to lead to higher performance boosts than enhancing set predictors. In particular, simple baselines such as training image representation backbones with binary cross-entropy have the potential to outperform other methods when combined with recent architec-

tural advancements for single label classification and given enough hyper-parameter search budget.

## 2. Overview of multi-label classification

Multi-label classification has been a long lasting problem in computer vision [72, 21, 73, 67] tackled by a wide variety of methods, such as, decomposing the problem into independent single-label classification problems [44, 72], exploiting label co-occurrences [1, 56, 34], introducing priors such as label noise and sparsity [21, 24, 58, 67, 73, 2], and more recently, by leveraging deep neural networks [69, 5, 61]. Approaches in the deep learning realm have also attempted to decompose the multi-label classification problem into single-label classification problems, by independently classifying features extracted from object proposals [69, 64, 35, 14] or by considering global image features and finetuning pre-trained models with a binary logistic loss [5, 4, 75, 16, 33]. In order to explicitly exploit label co-occurrences, researchers have resorted to modeling the joint probability distribution of labels [59] or decomposing the joint distribution into conditionals [11, 61, 45, 28, 32, 41, 46]. This has been done, for example, by using recurrent neural networks, at the expense of introducing intrinsic label ordering during training, which has been resolved by applying a category-wise max-pooling across the time dimension [62, 7, 71, 54] or by optimizing for the most likely ground truth label at each time step [6]. Alternative solutions to capture label co-occurrences include learning joint input-label embeddings with ranking-based losses [66, 31, 70, 29, 15], graph neural networks [8], and using loss functions that directly account for those [15, 63, 42, 54]. Finally, multi-label classification has only recently been posed as a set prediction problem, where both set elements (labels) and cardinality are predicted, e.g. [51, 52] model cardinality as a categorical distribution, [29] learns class-specific probability thresholds, and [65] frames set prediction as a parameterized policy search problem.

## 3. Benchmark methodology

In this section, we introduce our benchmark methodology. We start by reviewing the image-to-set prediction models, and follow by thoroughly describing the adopted hyper-parameter search strategy as well as the evaluation metric.

### 3.1. Image-to-set prediction models

In image-to-set prediction, we are given a dataset of image and set of labels pairs, with the goal of learning to produce the correct set of labels for a given image. The set of labels is an unordered collection of unique elements, which may have variable size. Let  $\mathcal{D} = \{d_i\}_{i=1}^N$  be a dictionary of labels of size  $N$ , from which we can obtain the set of labels  $S$  for an image  $\mathbf{x}$  by selecting  $K \geq 0$  elements from  $\mathcal{D}$ . If

$K = 0$ , no elements are selected and  $S = \{\}$ ; otherwise  $S = \{s_i\}_{i=1}^K$ . Thus, our training data consists of  $M$  image and label pairs  $\{(\mathbf{x}^{(i)}, S^{(i)})\}_{i=1}^M$ .

Image-to-set prediction models are composed of an *image representation* backbone, followed by a *set prediction* module, which are stacked together and trained end-to-end. Image representation backbones transform an input image  $\mathbf{x} \in \mathbb{R}^{W \times H \times 3}$  into a representation  $\mathbf{r} = f_\phi(\mathbf{x}) \in \mathbb{R}^{w \times h \times 2^{048}}$ , where  $W \times H$  and  $w \times h$  are the spatial resolutions of the image and its extracted features. Set prediction module takes as an input the image representation and outputs set elements. As *image representation* backbone, we choose the output of the last convolutional layer of a top performing convolutional network pre-trained on ImageNet [53]. In particular, we choose among popular image classification CNN architectures (ResNet-50 [18], ResNet-101 [18] and ResNeXt-101-32x8d [68]) to assess whether multi-label classification can also benefit from improvements in the single image classification literature. As *set predictor*, we consider feed-forward and auto-regressive architectures. A comprehensive overview of set predictor modules is out of the scope of this paper. We limit the scope of our study to assess the importance of design choices that (1) exploit *label co-occurrences* (either explicitly through model design or through the loss function), (2) leverage *label ordering* (e.g. auto-regressive models) and, (3) predict *set cardinality* as part of their pipeline (either through a categorical output, or an end-of-sequence – *eos* – token). Figure 1a summarizes the image-to-set prediction models considered in this study.

#### 3.1.1 Feed-forward Set Predictors

**Notation.** We represent  $S$  as a binary vector  $\mathbf{s}$  of dimension  $N$ , where  $s_i = 1$  if  $s_i \in S$  and 0 otherwise. The goal is to estimate the label probabilities  $\hat{\mathbf{s}}$  from an image  $\mathbf{x}$ .

**Architectures.** Feed-forward models take image features  $\mathbf{r}$  as input and output  $\hat{\mathbf{s}} = g_\theta(\mathbf{r})$ . These models are composed of (1) an optional  $1 \times 1$  convolutional block to change the feature dimensionality of the input, (2) a global average pooling operation to collapse the spatial dimensions, and (3) one or more fully connected layers. Intermediate fully connected layers are followed by dropout, batch normalization and a ReLU non-linearity. The last fully connected layer serves as classifier, and thus, is followed by either a sigmoid or softmax non-linearity. The architecture used for all feed-forward models is depicted in Figure 1b.

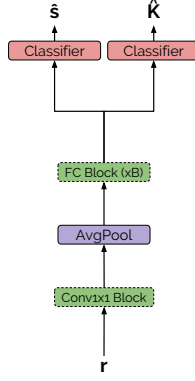
**Loss functions.** The model’s parameters are trained by maximizing:

$$\arg \max_{\phi, \theta} \sum_{i=0}^M \log p(\hat{\mathbf{s}}^{(i)} = \mathbf{s}^{(i)} | \mathbf{x}^{(i)}; \phi, \theta). \quad (1)$$

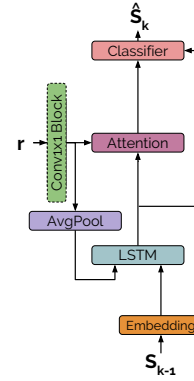
where  $\phi$  and  $\theta$  are the image representation and set predictor

Model	loss	co-occurrences	cardinality	ordering
FF	BCE	✗	✗	✗
FF	sIoU	ℒ	✗	✗
FF	TD	ℒ	✗	✗
FF	BCE	✗	DC dist.	✗
FF	BCE	✗	C dist.	✗
FF	sIoU	ℒ	C dist.	✗
FF	TD	ℒ	C dist.	✗
LSTM	CE	$\theta$	<i>eos</i> token	✓
LSTM <sub>set</sub>	BCE	$\theta$	<i>eos</i> token	✗
TF	CE	$\theta$	<i>eos</i> token	✓
TF <sub>set</sub>	BCE	$\theta$	<i>eos</i> token	✗

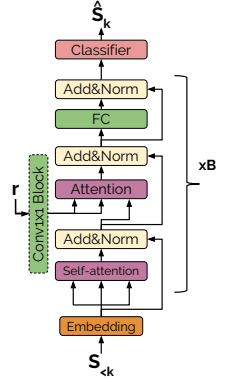
(a)



(b)



(c)



(d)

Figure 1: **(a) Models summary:** Loss-based modeling of label co-occurrences is denoted with  $\mathcal{L}$ , while explicitly modeling dependencies through architecture design is represented by  $\theta$ . Notation: FF (feed-forward), LSTM (long short-term memory), TF (transformer), BCE (binary cross-entropy), sIoU (soft intersection-over-union), TD (target distribution), CE (categorical cross-entropy), DC dist. (Dirichlet-Categorical) and C dist. (Categorical distribution). **(b–d) Set prediction architectures:** (b) Feed-forward (FF), (c) LSTM [38] and (d) Transformer [60].

parameters, respectively. Most state-of-the-art feed-forward methods assume independence among labels, factorizing  $\log p(\hat{\mathbf{s}}^{(i)} = \mathbf{s}^{(i)} | \mathbf{x}^{(i)})$  as  $\sum_{j=0}^N \log p(\hat{s}_j^{(i)} = s_j^{(i)} | \mathbf{x}^{(i)})$  and using binary cross-entropy (BCE) as training loss. However, the elements in the set are not necessarily independent. In order to account for label co-occurrences, we borrow from the semantic segmentation literature and train the feed-forward set predictor with a soft structured prediction loss, such as the *soft intersection-over-union* (sIoU) [12]. Alternatively, we use the *target distribution* (TD) [15, 42] to model the joint distribution of set elements and train a model by minimizing the cross-entropy loss between  $p(\mathbf{s}^{(i)} | \mathbf{x}^{(i)}) = \mathbf{s}^{(i)} / \sum_j \mathbf{s}_j^{(i)}$  and the model’s output distribution  $p(\hat{\mathbf{s}}^{(i)} | \mathbf{x}^{(i)})$ . We refer to the feed-forward models trained with the aforementioned losses as  $\text{FF}_{\text{BCE}}$ ,  $\text{FF}_{\text{sIoU}}$ , and  $\text{FF}_{\text{TD}}$ , respectively. Note that, by construction, none of these models exploit label ordering.

**Set cardinality.** Given the probabilities  $\hat{\mathbf{s}}$  estimated by a feed forward model, a set of labels  $\hat{S}$  must be recovered. For  $\text{FF}_{\text{BCE}}$  and  $\text{FF}_{\text{sIoU}}$ , one simple solution is to apply a threshold  $t$  to  $\hat{\mathbf{s}}$ , keeping all labels for which  $\hat{s}_i \geq t$ . Typically, this threshold is set to 0.5. Nonetheless, in the case of the  $\text{FF}_{\text{TD}}$ , we adopt the strategy of [54] and recover the label set by greedily sampling elements from a *cumulative distribution of sorted output probabilities*  $p(\hat{\mathbf{s}}^{(i)} | \mathbf{x}^{(i)})$ . We stop the sampling once the sum of probabilities of selected elements is  $> 0.5$ . Alternatively, the set cardinality  $K$  may be explicitly predicted by the feed-forward model through a second output  $\{\hat{\mathbf{s}}, \hat{K}\} = g_\theta(\mathbf{r})$ , where  $\hat{K}$  estimates the probabilities over possible set cardinalities. At inference time, the top- $\hat{K}$  labels are included in the predicted set.

We refer to these models as  $\text{FF}_{\text{BCE,C}}$ . For completeness, we also consider a variant of  $\text{FF}_{\text{BCE}}$  where the set cardinality is modeled with a Dirichlet-Categorical distribution ( $\text{FF}_{\text{BCE,DC}}$ ), following [52].

**Empty set prediction.** Unlabeled images can be naturally handled by models, whose output estimates a probability per label (e.g.  $\text{FF}_{\text{BCE}}$  and  $\text{FF}_{\text{sIoU}}$ ). At inference time, the set cardinality is determined by applying a threshold  $t$  to each output probability. The set cardinality can also be explicitly predicted by a feed-forward model through a second output, where the output of cardinality 0 corresponds to empty set. From the feed-forward models considered, only  $\text{FF}_{\text{TD}}$  cannot handle empty sets, since a vector with all zeros is not a valid (categorical) probability distribution.

### 3.1.2 Auto-regressive Set Predictors

**Notation.** We represent  $S$  as a  $K \times N$  binary matrix  $\mathbf{S}$ . We set  $\mathbf{S}_{i,j} = 1$  if label  $d_j$  is selected at  $i$ -th position and 0 otherwise. Each row in  $\mathbf{S}$  contains the one-hot-code representation of one label.

**Architectures.** We explore two auto-regressive architectures: a Long Short-Term Memory (LSTM) [20] with spatial attention-based model [38] and a transformer-based one (TF) [60]. Both architectures take image features  $\mathbf{r}$  as input and output  $\hat{\mathbf{S}} = g_\theta(\mathbf{r})$ . These models are composed of either a single LSTM layer – following [38] –, or several transformer layers – following [60] and [54]. The output layer of the model is used as classifier and has a softmax non-linearity. These models sequentially predict set labels. Their architectures are depicted in Figures 1c and 1d.

**Loss functions.** The models’ parameters are trained to predict  $\hat{\mathbf{S}}$  from an image  $\mathbf{x}$  by maximizing:

$$\arg \max_{\phi, \theta} \sum_{i=0}^M \log p(\hat{\mathbf{S}}^{(i)} = \mathbf{S}^{(i)} | \mathbf{x}^{(i)}; \phi, \theta). \quad (2)$$

To ensure that labels in  $\hat{\mathbf{S}}^{(i)}$  are selected without repetition, we force the pre-activation of  $p(\hat{\mathbf{S}}_k^{(i)} | \mathbf{x}^{(i)}, \mathbf{S}_{<k}^{(i)})$  to be  $-\infty$  for all previously selected labels. One characteristic of the formulation in Equation 2 is that it inherently exploits label ordering, which might not necessarily be relevant for the set prediction task. In order to ignore the order in which labels are predicted, we employ the solution of [62], [7] and [54], and aggregate the outputs across different time-steps by means of a max pooling operation. In this case, instead of minimizing the cross-entropy error at each time step, we minimize the BCE between the pooled predicted labels and the ground truth. We refer to the LSTM and TF models trained with pooled time-steps as  $\text{LSTM}_{\text{set}}$  and  $\text{TF}_{\text{set}}$ , respectively. It is worth noting that, in all cases, at inference time, we directly sample from the auto-regressive predictor’s output. As an alternative to prevent auto-regressive models from exploiting label ordering, we also consider a variant where we randomly shuffle the label ordering of each sample ( $\text{LSTM}_{\text{shuffle}}$  and  $\text{TF}_{\text{shuffle}}$ ).

**Set cardinality.** Most auto-regressive set predictors in the literature are not concerned with cardinality prediction, and predict a fixed number of labels by default [7, 61]. However, we argue that those models inherently have the mechanism to learn when to stop. Therefore, as commonly done in tasks such as image captioning and machine translation, we incorporate an *eos* token, which has to be predicted in the last sequence step. Thus, the *eos* token’s role is to estimate the cardinality of the set. In the case of  $\text{LSTM}_{\text{set}}$  and  $\text{TF}_{\text{set}}$ , we learn the stopping criterion with an additional loss weighted by means of a hyperparameter  $\lambda_{\text{eos}}$ . The *eos* loss is defined as the BCE between the predicted *eos* probability at different time-steps and the ground truth.

**Empty set prediction.** We handle images with missing labels by setting the *eos* token as the first element to be predicted in the sequence.

### 3.2. Hyper-parameter search

To warrant that differences in model performances can be attributed to modeling choices, we ensure that all models have an equal opportunity to shine by granting each one of them the same hyperparameter search budget through the HYPERBAND [27] algorithm. HYPERBAND is a bandit-based algorithm that speeds up random search via a more robust variant of the SUCCESSIVEHALVING early-stopping algorithm [22]. We have opted for HYPERBAND because it is extremely parallelizable, extensive evaluation has shown it achieves similar performance to more complex meth-

ods [27], and it has theoretical guarantees that do not rely on strong assumptions about the function to be optimized (in our case best overall F1 validation set score).

### 3.3. Evaluation protocol

We evaluate methods by means of F1 score that combines both precision and recall in a single score. For each tested model, we report three F1 values: per-class (C-F1), per-image (I-F1) and overall (O-F1).

## 4. Experiments

We ensure proper comparison among models by considering unified dataset splits and evaluate our models on 5 different datasets. Among those, we consider Pascal VOC 2007, MS COCO, and NUS-WIDE (following previous work but unifying dataset splits). Pascal VOC 2007 and MS COCO are object detection datasets and, as such, contain partially or fully visible objects exclusively. This is not the case of NUS-WIDE, which also contains concepts with higher degree of abstraction. However, all the aforementioned datasets have a rather limited dictionary size (below 100) and a small number of annotations per image ( $< 3$  on average). In the quest for pushing the boundaries of image-to-set prediction methods, we incorporate ADE20k [74] and Recipe1M [55] datasets to our analysis, since they exhibit significantly larger dictionary sizes (150 and 1496 vs  $< 100$ ) and greater number of annotations per image (8 on average). Moreover, Recipe1M includes image annotations corresponding to invisible items. Please refer to Table 2 and Figure 2 for additional dataset information. A detailed description of each dataset and HYPERBAND tuning parameters are provided in the supplementary material.

### 4.1. Analysis of set predictors

In this subsection, we aim to analyze the influence of the set predictor design. Table 3 reports results for 13 set predictors built on top of a ResNet-50 image representation backbone. Each experiment was run with 5 different seeds (different from the one used for hyper-parameter selection). Models appear ranked following their average normalized O-F1 score over all datasets (O-F1 scores are normalized using the maximum O-F1 of the corresponding dataset). Interestingly, the simplest baseline  $\text{FF}_{\text{BCE}}$  consistently exhibits close to top performance across datasets. In particular, the baseline models shine in COCO, NUS-WIDE and ADE20k datasets. Auto-regressive models (LSTM, TF and their shuffled versions) also rank favorably across most datasets, highlighting the potential role of modeling label co-occurrences. Moreover, their results suggests that, when there is an intrinsic label ordering in the dataset (e.g. NUS-WIDE and ADE20k preserve label order across dataset samples), exploiting it leads to increased performance. These findings raise the question of whether there

	VOC	COCO	NUS-WIDE	ADE20k	Recipe1M
Train	4 509	74 503	145 610	18 176	252 547
Val	502	8 280	16 179	2 020	5 000
Test	4 952	40 504	107 859	2 000	54 506
$N$	20	80	81	150	1 486
$K$	1.57 (0.77)	2.91 (1.84)	1.86 (1.71)	8.17 (4.14)	7.99 (3.21)

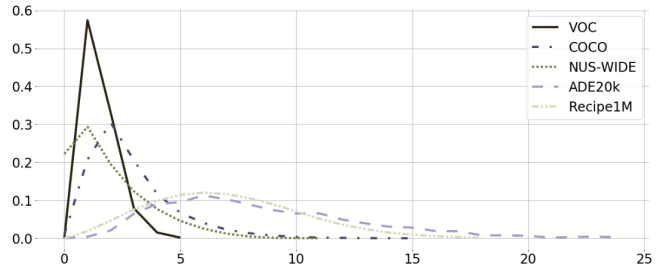


Figure 2: Dataset cardinality distribution.

Table 2: **Dataset summary.** Splits, dictionary size ( $N$ ), and cardinality ( $K$ ), reported as *mean (std)* for each dataset.

Rank	Model	VOC			COCO			NUS-WIDE			ADE20k			Recipe1M		
		O-F1	C-F1	I-F1	O-F1	C-F1	I-F1	O-F1	C-F1	I-F1	O-F1	C-F1	I-F1	O-F1	C-F1	I-F1
1	FF <sub>BCE</sub>	86.40 (0.19)	85.16 (0.20)	88.23 (0.15)	76.98 (0.06)	73.49 (0.14)	79.35 (0.07)	<b>71.34</b> <b>(0.06)</b>	<b>54.94</b> <b>(0.48)</b>	69.19 (0.12)	70.89 (0.34)	47.87 (1.28)	69.43 (0.30)	46.83 (0.07)	18.38 (0.17)	43.63 (0.07)
2	LSTM	86.36 (0.18)	85.00 (0.20)	88.20 (0.19)	76.63 (0.08)	72.98 (0.07)	79.45 (0.09)	70.85 (0.07)	54.15 (0.16)	<b>69.43</b> <b>(0.04)</b>	70.68 (0.23)	<b>48.73</b> <b>(1.40)</b>	69.97 (0.23)	47.33 (0.05)	17.55 (0.05)	46.12 (0.06)
3	TF	85.89 (0.16)	84.28 (0.26)	87.87 (0.16)	76.62 (0.11)	73.32 (0.12)	79.45 (0.07)	70.30 (0.06)	53.31 (0.45)	69.08 (0.07)	70.46 (0.15)	48.03 (0.51)	69.42 (0.25)	47.77 (0.07)	17.93 (0.07)	46.58 (0.08)
4	FF <sub>BCE,C</sub>	84.59 (0.14)	84.04 (0.18)	86.74 (0.18)	75.40 (0.06)	72.23 (0.13)	78.16 (0.08)	69.61 (0.05)	52.14 (0.72)	67.63 (0.29)	70.19 (0.13)	44.15 (0.47)	69.20 (0.13)	<b>50.22</b> <b>(0.03)</b>	18.28 (0.07)	<b>48.47</b> <b>(0.04)</b>
5	TF <sub>shuffle</sub>	86.79 (0.25)	85.62 (0.18)	88.63 (0.22)	77.04 (0.05)	73.72 (0.03)	79.99 (0.04)	69.51 (0.19)	52.74 (0.25)	68.23 (0.15)	70.26 (0.25)	45.71 (1.08)	69.47 (0.24)	46.78 (0.09)	18.94 (0.12)	45.62 (0.11)
6	FF <sub>TD,C</sub>	84.77 (0.10)	83.61 (0.26)	87.03 (0.08)	74.99 (0.08)	71.90 (0.14)	78.11 (0.05)	69.09 (0.10)	51.33 (0.84)	67.52 (0.36)	69.35 (0.13)	48.12 (0.27)	68.48 (0.19)	49.87 (0.10)	<b>18.96</b> <b>(0.35)</b>	48.39 (0.13)
7	LSTM <sub>shuffle</sub>	<b>87.45</b> <b>(0.27)</b>	<b>86.06</b> <b>(0.52)</b>	89.16 (0.26)	<b>77.11</b> <b>(0.09)</b>	73.56 (0.11)	<b>80.02</b> <b>(0.09)</b>	68.26 (0.13)	48.21 (1.60)	64.29 (0.72)	69.49 (0.20)	42.95 (0.62)	69.01 (0.20)	46.04 (0.12)	16.21 (0.11)	44.61 (0.13)
8	LSTM <sub>set</sub>	85.41 (0.34)	84.60 (0.37)	87.32 (0.35)	76.52 (0.08)	<b>73.83</b> <b>(0.12)</b>	78.98 (0.09)	69.82 (0.52)	53.82 (0.47)	67.83 (0.23)	69.42 (0.59)	46.25 (1.94)	68.64 (0.43)	46.68 (1.05)	18.85 (0.23)	45.28 (0.93)
9	TF <sub>set</sub>	86.26 (0.51)	85.10 (0.55)	88.05 (0.42)	59.74 (32.58)	56.80 (31.76)	61.70 (34.01)	70.18 (0.11)	53.70 (0.85)	67.59 (0.28)	<b>70.99</b> <b>(0.24)</b>	46.91 (0.45)	70.03 (0.26)	45.23 (4.40)	18.71 (1.69)	43.63 (4.38)
10	FF <sub>sIoU</sub>	87.25 (0.07)	85.92 (0.14)	<b>89.24</b> <b>(0.04)</b>	71.04 (0.50)	57.11 (1.47)	72.54 (0.76)	64.13 (1.45)	12.89 (0.47)	61.47 (5.96)	67.60 (0.17)	20.73 (0.40)	66.92 (0.19)	44.23 (0.35)	12.79 (0.04)	42.45 (0.33)
11	FF <sub>BCE,DC</sub>	85.77 (0.55)	84.11 (0.58)	87.82 (0.44)	70.63 (0.90)	66.94 (1.14)	72.19 (0.69)	61.54 (1.13)	44.23 (1.63)	59.66 (3.56)	70.75 (0.24)	46.03 (0.88)	<b>70.09</b> <b>(0.22)</b>	43.00 (3.05)	14.87 (1.25)	40.92 (3.22)
12	FF <sub>sIoU,C</sub>	85.89 (0.08)	84.31 (0.22)	88.01 (0.10)	67.62 (0.43)	50.66 (1.95)	68.97 (0.73)	63.12 (0.38)	12.56 (0.71)	63.69 (0.39)	65.90 (0.19)	19.88 (0.31)	65.02 (0.18)	42.78 (0.25)	12.69 (0.02)	40.69 (0.25)
13	FF <sub>TD</sub>	79.36 (0.22)	78.43 (0.32)	83.02 (0.18)	-	-	-	-	-	-	64.73 (0.37)	39.71 (0.78)	64.56 (0.33)	47.86 (0.04)	18.34 (0.07)	47.90 (0.05)

Table 3: **Set predictor comparison.** Results on VOC, COCO, NUS-WIDE, ADE20k and Recipe1M (test set), reported in terms of C-F1, O-F1 and I-F1. Models are trained 5 times using different random seeds. We report *mean (std)* for each metric, model and dataset. Image representation backbone is fixed to ResNet-50. The models are ordered according to their average normalized O-F1 score computed over all five tested datasets. Note that FF<sub>TD</sub> is not considered to obtain the mean ranking, since it is not used for datasets including empty sets. Note that these results are not directly comparable with the ones from Table 1.

exists an optimal per dataset label ordering to exploit, and support previous research along these lines [45, 6].

Taking a closer look at each dataset, the VOC top 3 performers across all metrics are LSTM<sub>shuffle</sub>, FF<sub>sIoU</sub> and TF<sub>shuffle</sub>, all of which model label co-occurrences. Among the least performing models, we find FF<sub>TD</sub> and all feed-forward models predicting set cardinality. These results suggest that modeling co-occurrences is beneficial,

while exploiting label ordering and predicting set cardinality seems less impactful. The COCO top 3 performers are LSTM<sub>shuffle</sub>, TF<sub>shuffle</sub> and FF<sub>BCE</sub>, which are closely followed by LSTM and TF (all within 1% difference from the top performer). Again, among the least performing models, we find most of the feed-forward models which explicitly predict the set cardinality.<sup>2</sup> In this case, exploit-

<sup>2</sup>The low performance and high variance of TF<sub>set</sub> is due to 2/5 seeds

ing label ordering becomes more challenging as COCO labels only follow partial ordering. For NUS-WIDE and ADE20k, top performers across all metrics also include auto-regressive models and  $FF_{BCE}$ . As previously mentioned, those datasets have an pre-established label ordering, which favors LSTM and TF models vs their shuffled counterparts. By contrast to other datasets, endowing feed-forward models with cardinality prediction seems to achieve good performance in ADE20k. Finally, Recipe1M presents slightly different trends, with auto-regressive models among mid-performers. The top performers across all metrics are  $FF_{BCE,C}$  and  $FF_{TD,C}$ , still advocating for the importance of cardinality prediction in feed-forward models when the dataset’s dictionary size is large.

Figure 3 presents the cardinality prediction errors for the 7 best models of Table 3. As shown in the figure, the average cardinality error grows with the dataset’s dictionary size, with VOC being the easiest dataset and Recipe1M the hardest. For Ade20k and Recipe1M datasets, feed-forward models explicitly trained to predict set cardinality (e. g. see  $FF_{BCE}$  vs.  $FF_{BCE,C}$ ) tend to be more accurate whereas for auto-regressive models, label shuffling leads to higher cardinality errors (e. g. see  $LSTM_{shuffle}$  vs LSTM). Although an explicit cardinality prediction reduces the cardinality error, it does not always translate into better label prediction results, as highlighted in Table 3.

Moreover, it is worth noting that all models report significantly lower values for C-F1 than for the rest of the metrics in the case of NUS-WIDE, ADE20k and Recipe1M. These drops can be explained by the low class frequencies exhibited by a large number of classes (long-tail class distribution), which result in low average C-F1 when looking at low-frequency classes (with relatively large variance).

## 4.2. Impact of the image representation backbone

In this subsection, we aim to assess the importance of the chosen image representation backbone. We compare the previously chosen ResNet-50 [18] to ResNet-101 [18] and ResNeXt-101-32x8d [68] for the 2 top ranked set predictors  $FF_{BCE}$  and LSTM. Table 4 reports the obtained results averaged across 5 different seeds (different from the one used for hyper-parameter selection in HYPERBAND). As shown in the table, for both set predictors, changing the image representation backbone from ResNet-50 to ResNet-101 or ResNeXt-101-32x8d leads to improvements in terms of all F1 scores. Improvements are especially notable for the  $FF_{BCE}$  set predictor, which gains over 1% points in O-F1 in 4 out of 5 datasets, leading to a boost in performance when compared to the best models of Table 3. We hypothesize that feed forward predictors benefit more from enhanced single-label image classification backbones given their model design. Both single-label image classifiers and

that did not converge.

feed forward set predictors are composed of fully connected layers that are stacked on top of their respective convolutional backbones. As such, improvements in single-label image classification backbones translate into improvements in the multi-label scenario. Figures 4a and 4b highlight the O-F1 improvement that the best set predictor of Table 3 achieves with respect to  $FF_{BCE}$  and LSTM respectively, for a fixed ResNet-50 image representation backbone. Similarly, the figure also displays the O-F1 improvement obtained when changing the image representation backbone of the same set predictors ( $FF_{BCE}$  and LSTM). Interestingly, when it comes to  $FF_{BCE}$ , exploiting better image representation backbones leads to higher improvements than enhancing the set predictor module while fixing the image representation backbone to ResNet-50. This observation also holds in 3 out of 5 datasets in the case of the LSTM set predictor, which exhibits larger margins of improvement when changing the image representation backbone rather than the set predictor itself.

## 4.3. Summary of observations

On the one hand, our experiments have shown that image-to-set prediction backbones follow the trends of single label classification, i.e. ResNext-101 improving results over both ResNet-50 and ResNet-101. Moreover, our results suggest that, in many cases, enhancing the image representation backbone can provide larger performance boosts than enhancing the set predictors. Therefore, when designing new image-to-set prediction models, we recommend taking advantage of the top performing single-label classification architectures.

On the other hand, when it comes to set predictors, auto-regressive models which explicitly leverage label co-occurrences seem to achieve slightly better overall results. In that case, exploiting dataset order is beneficial for datasets that consistently present labels following the same order. Including cardinality prediction in feed forward models seems to be relevant in cases where the dictionary size is very large (e.g. in Recipe1M). One must not disregard the high performance achieved by the simple yet effective baseline model, namely  $FF_{BCE}$ , which has the potential to achieve the best performing results when given the best image representation backbone.

Finally, it is important to note that we experienced a significant performance boost (in all methods) when employing an automatic hyper-parameter strategy. In this case, it is important to allocate the same search budget to all models and baselines to ensure a fair comparison and robust conclusions on the proposed approach.

## 5. Conclusion

In this paper, we have described important reproducibility challenges in the image-to-set prediction literature that

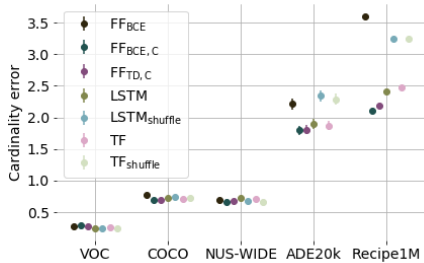
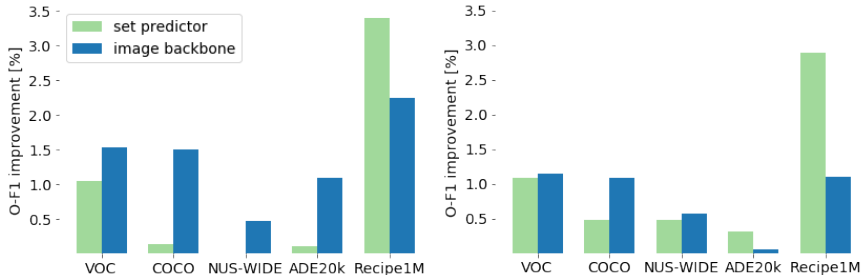


Figure 3: **Cardinality error per image (mean and 95% confidence interval).** We compare the top 7 models from Table 3.



(a) Comparison based on  $FF_{BCE}$

(b) Comparison based on LSTM

Figure 4: **O-F1 improvements when changing set predictor vs. image representation backbone.**

Model	Backbone	VOC			COCO			NUS-WIDE			ADE20k			Recipe1M		
		O-F1	C-F1	I-F1	O-F1	C-F1	I-F1	O-F1	C-F1	I-F1	O-F1	C-F1	I-F1	O-F1	C-F1	I-F1
$FF_{BCE}$	ResNet-50	86.40 (0.19)	85.16 (0.20)	88.23 (0.15)	76.98 (0.06)	73.49 (0.14)	79.35 (0.07)	71.34 (0.06)	54.94 (0.48)	69.19 (0.12)	70.89 (0.34)	47.87 (1.28)	69.43 (0.30)	46.83 (0.07)	18.38 (0.17)	43.63 (0.07)
	ResNet-101	87.64 (0.14)	86.57 (0.23)	89.34 (0.12)	77.67 (0.07)	74.78 (0.11)	79.80 (0.10)	<b>71.81</b> (0.04)	57.82 (0.07)	<b>69.61</b> (0.09)	71.81 (0.23)	<b>49.92</b> (0.60)	70.81 (0.22)	47.90 (0.12)	18.59 (0.11)	44.78 (0.12)
	ResNeXt-101-32x8d	<b>87.93</b> (0.20)	<b>87.60</b> (0.13)	<b>90.05</b> (0.18)	<b>78.48</b> (0.09)	<b>75.62</b> (0.19)	<b>80.88</b> (0.12)	71.72 (0.02)	<b>57.95</b> (0.10)	69.34 (0.03)	<b>71.98</b> (0.21)	46.25 (0.44)	<b>70.87</b> (0.24)	<b>49.07</b> (0.10)	<b>19.13</b> (0.02)	<b>46.12</b> (0.12)
LSTM	ResNet-50	86.36 (0.18)	85.00 (0.20)	88.20 (0.09)	76.63 (0.08)	72.98 (0.07)	79.45 (0.09)	70.85 (0.07)	54.15 (0.16)	69.43 (0.04)	70.68 (0.23)	<b>48.73</b> (1.40)	69.97 (0.23)	47.33 (0.05)	17.55 (0.05)	46.12 (0.06)
	ResNet-101	87.29 (0.32)	85.77 (0.43)	89.01 (0.31)	77.62 (0.06)	74.39 (0.12)	80.27 (0.07)	<b>71.43</b> (0.03)	<b>55.76</b> (0.24)	<b>70.08</b> (0.04)	<b>70.73</b> (0.11)	48.13 (0.41)	<b>70.06</b> (0.20)	48.03 (0.07)	17.87 (0.05)	46.84 (0.08)
	ResNeXt-101-32x8d	<b>87.51</b> (0.16)	<b>86.53</b> (0.16)	<b>89.40</b> (0.18)	<b>77.71</b> (0.07)	<b>74.74</b> (0.12)	<b>80.34</b> (0.08)	70.86 (0.16)	54.26 (0.36)	69.58 (0.23)	70.00 (0.20)	47.84 (1.14)	69.23 (0.29)	<b>48.43</b> (0.06)	<b>18.18</b> (0.15)	<b>47.23</b> (0.08)

Table 4: **Image representation backbone comparison.** Results on VOC, COCO, NUS-WIDE, ADE20k and Recipe1M (test set) reported in terms of C-F1, O-F1 and I-F1. Models are trained 5 times using different random seeds. We report *mean (std)* for each metric, set predictor, image representation backbone and dataset. Note that these results are not directly comparable with the ones from Table 1.

impede proper comparisons among published methods and hinder the research progress. To alleviate this issue, we equipped the community with a benchmark suite composed of a unified code-base, predefined splits for 5 datasets of increasing complexity and a common evaluation protocol to assess the impact of current design choices and future innovations. Together with the benchmark suite release, we performed an in-depth analysis of the key components of current image-to-set prediction models, namely the choice of image representation backbone as well as the set predictor design. In total, we compared 3 different image representation backbones and 13 different families of set predictors. To ensure fair and robust comparisons among methods, we used the HYPERBAND algorithm with a fixed budget of tested configurations (410 hyperparameter configurations evaluated per model) and reported results averaged over 5 different seeds (different than that used for tuning).

Looking forward, we expect that the release of the benchmark suite and the performed analysis will accelerate research in the image-to-set prediction domain, by en-

suring firm steps and robust conclusions out of future contributions. As general guidance, when introducing new set prediction approaches, we suggest:

- Initializing the image-to-set prediction backbone with ImageNet pre-trained models.
- Performing hyper-parameter search of the newly introduced methods by fixing a limited budget of configurations to be tested (and applying the same budget to baselines).
- Using the suggested validation set to perform architectural and optimization hyper-parameter search, including early-stopping.
- Checking the test set performance only once, after finalizing the hyper-parameter tuning.
- Reporting results on the test set with multiple image representation backbones and training seeds.

Together with the benchmark suite, we release a subset of the top performing models per dataset. These pre-trained models are meant to be used for future comparisons and, potentially, transfer learning.



## References

- [1] Alessandro Antonucci, Giorgio Corani, Denis Deratani Mauá, and Sandra Gabaglio. An ensemble of bayesian networks for multilabel classification. In *IJCAI*, 2013. 3
- [2] Wei Bi and James T. Kwok. Efficient multi-label classification with many labels. In *ICML*, 2013. 3
- [3] Xavier Bouthillier, César Laurent, and Pascal Vincent. Unreproducible research is reproducible. In Kamalika Chaudhuri and Ruslan Salakhutdinov, editors, *Proceedings of the 36th International Conference on Machine Learning*, volume 97 of *Proceedings of Machine Learning Research*, pages 725–734, Long Beach, California, USA, 09–15 Jun 2019. PMLR. 1
- [4] Ken Chatfield, Karen Simonyan, Andrea Vedaldi, and Andrew Zisserman. Return of the devil in the details: Delving deep into convolutional nets. *BMVC*, 2014. 3
- [5] Jing-Jing Chen and Chong-Wah Ngo. Deep-based ingredient recognition for cooking recipe retrieval. In *ACM Multimedia*, 2016. 3
- [6] Shang-Fu Chen, Yi-Chen Chen, Chih-Kuan Yeh, and Yu-Chiang Frank Wang. Order-free rnn with visual attention for multi-label classification. In *AAAI*, 2018. 2, 3, 6
- [7] Tianshui Chen, Zhouxia Wang, Guanbin Li, and Liang Lin. Recurrent attentional reinforcement learning for multi-label image recognition. In *AAAI*, 2018. 2, 3, 5
- [8] Zhao-Min Chen, Xiu-Shen Wei, Peng Wang, and Yanwen Guo. Multi-label image recognition with graph convolutional networks. In *CVPR*, 2019. 2, 3
- [9] Tat-Seng Chua, Jinhui Tang, Richang Hong, Haojie Li, Zhiping Luo, and Yantao Zheng. Nus-wide: a real-world web image database from national university of singapore. In *ACM Conference on Image and Video Retrieval*, 2009. 2, 12
- [10] Marius Cordts, Mohamed Omran, Sebastian Ramos, Timo Rehfeld, Markus Enzweiler, Rodrigo Benenson, Uwe Franke, Stefan Roth, and Bernt Schiele. The cityscapes dataset for semantic urban scene understanding. In *The IEEE Conference on Computer Vision and Pattern Recognition (CVPR)*, June 2016. 1
- [11] Krzysztof Dembczyński, Weiwei Cheng, and Eyke Hüllermeier. Bayes optimal multilabel classification via probabilistic classifier chains. In *ICML*, 2010. 3
- [12] Michal Drozdal, Eugene Vorontsov, Gabriel Chartrand, Samuel Kadoury, and Chris Pal. The importance of skip connections in biomedical image segmentation. In Gustavo Carneiro, Diana Mateus, Loïc Peter, Andrew Bradley, João Manuel R. S. Tavares, Vasileios Belagiannis, João Paulo Papa, Jacinto C. Nascimento, Marco Loog, Zhi Lu, Jaime S. Cardoso, and Julien Cornebise, editors, *Deep Learning and Data Labeling for Medical Applications*, pages 179–187, Cham, 2016. Springer International Publishing. 4
- [13] Mark Everingham, Luc Van Gool, Christopher KI Williams, John Winn, and Andrew Zisserman. The pascal visual object classes (voc) challenge. *IJCV*, 2010. 2, 12
- [14] Weifeng Ge, Sibe Yang, and Yizhou Yu. Multi-evidence filtering and fusion for multi-label classification, object detection and semantic segmentation based on weakly supervised learning. In *CVPR*, 2018. 2, 3
- [15] Yunchao Gong, Yangqing Jia, Thomas Leung, Alexander Toshev, and Sergey Ioffe. Deep convolutional ranking for multilabel image annotation. *CoRR*, abs/1312.4894, 2013. 3, 4
- [16] Hao Guo, Kang Zheng, Xiaochuan Fan, Hongkai Yu, and Song Wang. Visual attention consistency under image transforms for multi-label image classification. In *CVPR*, 2019. 2, 3
- [17] Kaiming He, Georgia Gkioxari, Piotr Dollár, and Ross Girshick. Mask r-cnn. In *ICCV*, 2017. 1
- [18] Kaiming He, Xiangyu Zhang, Shaoqing Ren, and Jian Sun. Deep residual learning for image recognition. In *CVPR*, 2016. 1, 3, 7
- [19] Peter Henderson, Riashat Islam, Philip Bachman, Joelle Pineau, Doina Precup, and David Meger. Deep reinforcement learning that matters. *CoRR*, abs/1709.06560, 2017. 1
- [20] Sepp Hochreiter and Jürgen Schmidhuber. Long short-term memory. *Neural computation*, 1997. 4
- [21] Daniel J Hsu, Sham M Kakade, John Langford, and Tong Zhang. Multi-label prediction via compressed sensing. In Y. Bengio, D. Schuurmans, J. D. Lafferty, C. K. I. Williams, and A. Culotta, editors, *NeurIPS*. Curran Associates, Inc., 2009. 3
- [22] Kevin Jamieson and Ameet Talwalkar. Non-stochastic best arm identification and hyperparameter optimization. In *AISTATS*, pages 240–248, 2016. 5
- [23] Simon Jégou, Michal Drozdal, David Vazquez, Adriana Romero, and Yoshua Bengio. The one hundred layers tiramisu: Fully convolutional densenets for semantic segmentation. In *CVPR-W*, 2017. 1
- [24] Ashish Kapoor, Raajay Viswanathan, and Prateek Jain. Multilabel classification using bayesian compressed sensing. In F. Pereira, C. J. C. Burges, L. Bottou, and K. Q. Weinberger, editors, *NeurIPS*. Curran Associates, Inc., 2012. 3
- [25] Diederik P. Kingma and Jimmy Ba. Adam: A method for stochastic optimization. *CoRR*, abs/1412.6980, 2014. 12
- [26] Karol Kurach, Mario Lucic, Xiaohua Zhai, Marcin Michalski, and Sylvain Gelly. The GAN landscape: Losses, architectures, regularization, and normalization. *CoRR*, abs/1807.04720, 2018. 1
- [27] Lisha Li, Kevin Jamieson, Giulia DeSalvo, Afshin Roshtamzadeh, and Ameet Talwalkar. Hyperband: A novel bandit-based approach to hyperparameter optimization. *JMLR*, 18(185):1–52, 2018. 2, 5
- [28] Liang Li, Shuhui Wang, Shuqiang Jiang, and Qingming Huang. Attentive recurrent neural network for weak-supervised multi-label image classification. In *ACM Multimedia*, 2018. 2, 3
- [29] Yuncheng Li, Yale Song, and Jiebo Luo. Improving pairwise ranking for multi-label image classification. In *CVPR*, 2017. 2, 3
- [30] Tsung-Yi Lin, Michael Maire, Serge Belongie, James Hays, Pietro Perona, Deva Ramanan, Piotr Dollár, and C Lawrence Zitnick. Microsoft coco: Common objects in context. In *ECCV*, 2014. 1, 2, 12

- [31] Zijia Lin, Guiguang Ding, Mingqing Hu, and Jianmin Wang. Multi-label classification via feature-aware implicit label space encoding. In *ICML*, 2014. 3
- [32] Feng Liu, Tao Xiang, Timothy M Hospedales, Wankou Yang, and Changyin Sun. Semantic regularisation for recurrent image annotation. In *CVPR*, 2017. 2, 3
- [33] Luchen Liu, Sheng Guo, Weilin Huang, and Matthew R Scott. Decoupling category-wise independence and relevance with self-attention for multi-label image classification. In *ICASSP*, 2019. 2, 3
- [34] Weiwei Liu and Ivor W. Tsang. Large margin metric learning for multi-label prediction. In *AAAI*, 2015. 3
- [35] Yongcheng Liu, Lu Sheng, Jing Shao, Junjie Yan, Shiming Xiang, and Chunhong Pan. Multi-label image classification via knowledge distillation from weakly-supervised detection. In *ACM Multimedia*, 2018. 2, 3
- [36] Francesco Locatello, Stefan Bauer, Mario Lucic, Sylvain Gelly, Bernhard Schölkopf, and Olivier Bachem. Challenging common assumptions in the unsupervised learning of disentangled representations. *CoRR*, abs/1811.12359, 2018. 1
- [37] Jonathan Long, Evan Shelhamer, and Trevor Darrell. Fully convolutional networks for semantic segmentation. In *CVPR*, 2015. 1
- [38] Jiasen Lu, Caiming Xiong, Devi Parikh, and Richard Socher. Knowing when to look: Adaptive attention via a visual sentinel for image captioning. In *CVPR*, 2017. 4
- [39] Mario Lucic, Karol Kurach, Marcin Michalski, Sylvain Gelly, and Olivier Bousquet. Are gans created equal? a large-scale study. In S. Bengio, H. Wallach, H. Larochelle, K. Grauman, N. Cesa-Bianchi, and R. Garnett, editors, *Advances in Neural Information Processing Systems 31*, pages 700–709. Curran Associates, Inc., 2018. 1
- [40] Yan Luo, Ming Jiang, and Qi Zhao. Visual attention in multi-label image classification. In *CVPR-W*, 2019. 2
- [41] Fan Lyu, Qi Wu, Fuyuan Hu, Qingyao Wu, and Mingkui Tan. Attend and imagine: Multi-label image classification with visual attention and recurrent neural networks. *IEEE Transactions on Multimedia*, 2019. 3
- [42] Dhruv Mahajan, Ross B. Girshick, Vignesh Ramanathan, Kaifeng He, Manohar Paluri, Yixuan Li, Ashwin Bharambe, and Laurens van der Maaten. Exploring the limits of weakly supervised pretraining. *CoRR*, abs/1805.00932, 2018. 3, 4
- [43] Gábor Melis, Chris Dyer, and Phil Blunsom. On the state of the art of evaluation in neural language models. *CoRR*, abs/1707.05589, 2017. 1
- [44] Jinseok Nam, Jungi Kim, Eneldo Loza Mencía, Iryna Gurevych, and Johannes Fürnkranz. Large-scale multi-label text classification — revisiting neural networks. In *ECMLP-KDD*, 2014. 3
- [45] Jinseok Nam, Eneldo Loza Mencía, Hyunwoo J Kim, and Johannes Fürnkranz. Maximizing subset accuracy with recurrent neural networks in multi-label classification. In *NeurIPS*, 2017. 3, 6
- [46] Nelson Nauata, Hexiang Hu, Guang-Tong Zhou, Zhiwei Deng, Zicheng Liao, and Greg Mori. Structured label inference for visual understanding. *TPAMI*, 2019. 3
- [47] Avital Oliver, Augustus Odena, Colin Raffel, Ekin D. Cubuk, and Ian J. Goodfellow. Realistic evaluation of deep semi-supervised learning algorithms. *CoRR*, abs/1804.09170, 2018. 1
- [48] Adam Paszke, Sam Gross, Soumith Chintala, Gregory Chanan, Edward Yang, Zachary DeVito, Zeming Lin, Alban Desmaison, Luca Antiga, and Adam Lerer. Automatic differentiation in pytorch. In *NeurIPS-W*, 2017. 13
- [49] Joseph Redmon, Santosh Divvala, Ross Girshick, and Ali Farhadi. You only look once: Unified, real-time object detection. In *CVPR*, 2016. 1
- [50] Shaoqing Ren, Kaifeng He, Ross Girshick, and Jian Sun. Faster R-CNN: towards real-time object detection with region proposal networks. In *NeurIPS*, 2015. 1
- [51] S Hamid Rezaatoughi, Anton Milan, Ehsan Abbasnejad, Anthony Dick, Ian Reid, et al. Deepsetnet: Predicting sets with deep neural networks. In *ICCV*, 2017. 2, 3
- [52] S Hamid Rezaatoughi, Anton Milan, Qinfeng Shi, Anthony Dick, and Ian Reid. Joint learning of set cardinality and state distribution. *AAAI*, 2018. 2, 3, 4
- [53] Olga Russakovsky, Jia Deng, Hao Su, Jonathan Krause, Sanjeev Satheesh, Sean Ma, Zhiheng Huang, Andrej Karpathy, Aditya Khosla, Michael Bernstein, Alexander C. Berg, and Li Fei-Fei. ImageNet Large Scale Visual Recognition Challenge. *IJCV*, 2015. 1, 3
- [54] Amaia Salvador, Michal Drozdal, Xavier Giró i Nieto, and Adriana Romero. Inverse cooking: Recipe generation from food images. In *CVPR*, 2019. 3, 4, 5, 12
- [55] Amaia Salvador, Nicholas Hynes, Yusuf Aytar, Javier Marin, Ferda Ofli, Ingmar Weber, and Antonio Torralba. Learning cross-modal embeddings for cooking recipes and food images. In *CVPR*, 2017. 2, 5, 12
- [56] Xin Shu, Darong Lai, Huanliang Xu, and Liang Tao. Learning shared subspace for multi-label dimensionality reduction via dependence maximization. *Neurocomputing*, 2015. 3
- [57] Karen Simonyan and Andrew Zisserman. Very deep convolutional networks for large-scale image recognition. In *ICLR*, 2015. 1
- [58] Yale Song, Daniel McDuff, Deepak Vasisht, and Ashish Kapoor. Exploiting sparsity and co-occurrence structure for action unit recognition. In *FG*. IEEE Computer Society, 2015. 3
- [59] Grigorios Tsoumakas and Ioannis Vlahavas. Random k-labelsets: An ensemble method for multilabel classification. In Joost N. Kok, Jacek Koronacki, Raomon Lopez de Mantaras, Stan Matwin, Dunja Mladenič, and Andrzej Skowron, editors, *ECML*, 2007. 3
- [60] Ashish Vaswani, Noam Shazeer, Niki Parmar, Jakob Uszkoreit, Llion Jones, Aidan N Gomez, Łukasz Kaiser, and Illia Polosukhin. Attention is all you need. In *NeurIPS*, 2017. 4
- [61] Jiang Wang, Yi Yang, Junhua Mao, Zhiheng Huang, Chang Huang, and Wei Xu. CNN-RNN: A unified framework for multi-label image classification. In *CVPR*, 2016. 2, 3, 5
- [62] Zhouxia Wang, Tianshui Chen, Guanbin Li, Ruijia Xu, and Liang Lin. Multi-label image recognition by recurrently discovering attentional regions. In *ICCV*, 2017. 2, 3, 5

- [63] Yunchao Wei, Wei Xia, Junshi Huang, Bingbing Ni, Jian Dong, Yao Zhao, and Shuicheng Yan. CNN: single-label to multi-label. *CoRR*, abs/1406.5726, 2014. 3
- [64] Yunchao Wei, Wei Xia, Min Lin, Junshi Huang, Bingbing Ni, Jian Dong, Yao Zhao, and Shuicheng Yan. Hcp: A flexible cnn framework for multi-label image classification. *TPAMI*, 2016. 3
- [65] Sean Welleck, Zixin Yao, Yu Gai, Jialin Mao, Zheng Zhang, and Kyunghyun Cho. Loss functions for multiset prediction. In S. Bengio, H. Wallach, H. Larochelle, K. Grauman, N. Cesa-Bianchi, and R. Garnett, editors, *Advances in Neural Information Processing Systems 31*, pages 5783–5792. Curran Associates, Inc., 2018. 3
- [66] Jason Weston, Samy Bengio, and Nicolas Usunier. Wsabie: Scaling up to large vocabulary image annotation. In *IJCAI*, 2011. 3
- [67] Baoyuan Wu, Fan Jia, Wei Liu, Bernard Ghanem, and Siwei Lyu. Multi-label learning with missing labels using mixed dependency graphs. *IJCV*, 2018. 3
- [68] Saining Xie, Ross Girshick, Piotr Dollár, Zhuowen Tu, and Kaiming He. Aggregated residual transformations for deep neural networks. In *CVPR*, 2017. 3, 7
- [69] Hao Yang, Joey Tianyi Zhou, Yu Zhang, Bin-Bin Gao, Jianxin Wu, and Jianfei Cai. Exploit bounding box annotations for multi-label object recognition. In *CVPR*, 2016. 3
- [70] Chih-Kuan Yeh, Wei-Chieh Wu, Wei-Jen Ko, and Yu-Chiang Frank Wang. Learning deep latent spaces for multi-label classification. *CoRR*, abs/1707.00418, 2017. 3
- [71] Junjie Zhang, Qi Wu, Chunhua Shen, Jian Zhang, and Jianfeng Lu. Multilabel image classification with regional latent semantic dependencies. *IEEE Transactions on Multimedia*, 2018. 2, 3
- [72] Min-Ling Zhang and Zhi-Hua Zhou. Ml-knn: A lazy learning approach to multi-label learning. *Pattern Recogn.*, 40(7), July 2007. 3
- [73] Feipeng Zhao and Yuhong Guo. Semi-supervised multi-label learning with incomplete labels. In *IJCAI*, 2015. 3
- [74] Bolei Zhou, Hang Zhao, Xavier Puig, Sanja Fidler, Adela Barriuso, and Antonio Torralba. Scene parsing through ade20k dataset. In *CVPR*, 2017. 2, 5, 12
- [75] Feng Zhu, Hongsheng Li, Wanli Ouyang, Nenghai Yu, and Xiaogang Wang. Learning spatial regularization with image-level supervisions for multi-label image classification. In *CVPR*, 2017. 2, 3

# Supplementary material

We start the supplementary material by providing a short description of the datasets used (Section A). Then, in Section B, we provide implementation details, including data pre-processing, hyperparameter values considered for the HYPERBAND tuning, as well as values of the selected hyperparameters.

## A. Datasets details

We train and evaluate our models on five different image datasets, which provide multi-label annotations.

**Pascal VOC 2007** [13] is a popular benchmark for image classification, object detection and segmentation tasks. It is composed of 9 963 images containing objects from 20 distinct categories. Images are divided in 2 501, 2 510 and 4 952 for train, validation and test splits, respectively. We train with 90% of the *trainval* images, keeping 10% for validation. Models are evaluated on the test set, for which annotations have been released.

**MS COCO 2014** [30] is a popular benchmark for object detection and segmentation on natural images, containing annotations for objects of 80 different categories. It is composed of 82 783 images for training and 40 504 for validation. Since evaluation on the test set can only be done through the benchmark server, which currently does not support the set prediction task, we use 10% of the training set for validation, and evaluate on the full validation set. Note that in our experiments we include images with no annotations as *empty sets*.

**NUS-WIDE** [9] is a web image database composed of 161 789 images for training and 107 859 for testing, annotated with 81 unique tags collected from Flickr. While VOC and MS COCO are annotated with visually grounded object tags (e.g. *dog*, *train* or *person*), NUS-WIDE includes a wider variety of tags referring to activities (e.g. *wedding*, *soccer*), scenes (e.g. *snow*, *airport*) and objects (e.g. *car*, *computer*, *dog*). As in COCO, this dataset includes images with *empty sets* annotations.

**ADE20k** [74] is a scene parsing dataset, containing 20 210 training, 2 000 validation samples, annotated with a dictionary of 150 labels. Since the test set server evaluation is not suited for image to set prediction, we use validation set as a test set and separate a new validation set from the training set. As a result we obtain 18 176, 2 020 and 2 000 images for train, validation and test splits, respectively.

**Recipe1M** [55] composed of 1 029 720 recipes scraped from cooking websites. The dataset is split in 720 639 training, 155 036 validation and 154 045 test samples, each containing a cooking recipe (from which we only use ingredients) and (optionally) images. In our experiments, we use only those samples containing images. Following [54], we pre-process the ingredient dictionary by (1) removing plurals, (2) clustering together ingredients that share the first or last two words, (3) merge ingredients sharing the first or last word, (4) removing infrequent ingredients (appearing less than 10 times), and (5) remove recipes with less than 2 ingredients. This procedure results in 1 486 unique ingredients and 252 547 training, 54 255 validation and 54 506 test samples. To speed up the training, we use 5 000 randomly chosen validation images.

### A.1. Order in dataset labels

In this Subsection, we demonstrate that some datasets come with a preexisting label order while other do not. Figure 5 depicts the order in label pairs for each dataset. The x-axis is normalized for each dataset. For each label pair ( $A$ ,  $B$ ), we compute the number of times that one label precedes the other. Then, we compute order  $O = \max(a, b)/(a + b)$ , where  $a$  accounts for the number of times that  $A$  precedes  $B$  in the set (and vice versa for  $b$ ). A value of  $O = 0.5$  indicates no order (i.e.  $A$  precedes  $B$  as often as  $B$  precedes  $A$ ), and a value of 1.0 indicates total order ( $A$  always precedes  $B$ , or vice versa). In the case of NUS-WIDE and ADE20k, labels always appear in the same order for all datapoints. For VOC, COCO and Recipe1M, while the plot reveals some degree of order for all label pairs (all values are above 0.5), most values are below 1.0, indicating that label order is not consistent across samples.

## B. Implementation details

### B.1. Data pre-processing

We resize all images to 448 pixels in their shortest side, preserving aspect ratio, and take random crops of  $448 \times 448$  for training. We randomly flip ( $p = 0.5$ ), translate (within a range of  $\pm 10\%$  of the image size on each axis) and rotate images ( $\pm 10^\circ$ ) for data augmentation during training. All models are trained with the Adam optimizer [25] for a maximum of 200 epochs, or until early-stopping criterion is met (monitoring the O-F1 metric and using patience of 50 epochs for VOC and 10 epochs for the remaining datasets).

\*Equal contribution.

†Work partially done during internship at Facebook AI Research.

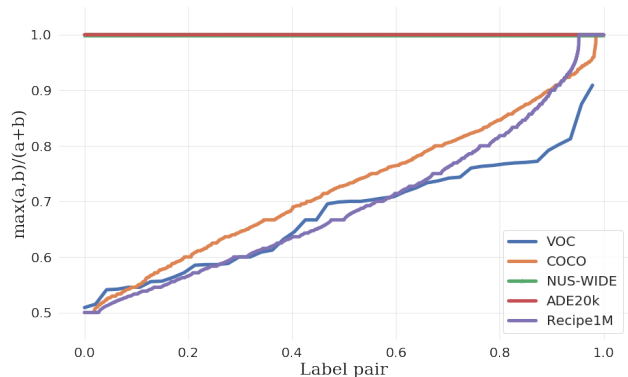


Figure 5: **Order in label pairs.**

All models are implemented with PyTorch<sup>1</sup> [48]. For autoregressive models, we train on two variants of annotations: (1) we keep the dataset order (e. g. LSTM and TF), and (2) we randomly shuffle the labels each time we load an image (e. g. LSTM<sub>shuffle</sub> and TF<sub>shuffle</sub>).

## B.2. Hyperband details

The operation of HYPERBAND is controlled by two hyperparameters. One,  $\eta$ , controls the aggressiveness of the algorithm, by specifying the ratio of configurations that are kept after each round (the best  $1/\eta$  hyperparameters are kept). The other,  $R$ , controls the maximum number of resources (e.g., epochs) that can be spent by configuration, as well as the total number of configurations to evaluate. In our experiments, we used  $\eta = 3$  and  $R = 600$ , where each resource unit is equivalent to 0.15 training epochs for most datasets (0.2 epochs for VOC)<sup>2</sup>, rounding up when necessary. This translates to 410 hyperparameter configurations evaluated per model, and a maximum budget of 3 200 epochs (4 400 for VOC) for the complete tuning process (with at most 90 training epochs per model).

For hyperparameter tuning, we allowed HYPERBAND to sample values from a set of mutually independent categorical distributions, one for each hyperparameter. The hyperparameters considered for all models, and their possible values, are shown in Tables 5 and 6. The hyperparameter values corresponding to the best models found by HYPERBAND for each dataset are shown in Tables 7-11.

<sup>1</sup><http://pytorch.org/>

<sup>2</sup>As VOC is a smaller dataset, we set a larger maximum number of epochs to allow more gradient updates to all models.

Hyperparameter	Values
Embedding size	[256, 512, 1 024, 2 048]
Learning rate	$[10^{-4}, 10^{-3}, 10^{-2}]$
Image encoder’s learning rate scale	$[10^{-2}, 10^{-1}]$
Dropout rate	[0, 0.1, 0.3, 0.5]
Weight decay	$[0, 10^{-4}]$

Table 5: Hyperparameters common to all models and their possible values.

Models	$L_t$	$L_f$	$n_{att}$	$\lambda_C$	$\lambda_{eos}$
TF, TF <sub>shuffle</sub>	[1, 2, 3]	–	[2, 4, 8]	–	–
TF <sub>set</sub>	[1, 2, 3]	–	[2, 4, 8]	–	$[10^{-3}, 10^{-2}, 10^{-1}, 0.5, 1, 10, 100]$
LSTM <sub>set</sub>	–	–	–	–	$[10^{-3}, 10^{-2}, 10^{-1}, 0.5, 1, 10, 100]$
FF <sub>BCE</sub> , FF <sub>TD</sub> , FF <sub>sIoU</sub>	–	[0, 1, 2, 3]	–	–	–
FF <sub>BCE,DC</sub>	–	[0, 1, 2, 3]	–	1	–
FF <sub>BCE,C</sub> , FF <sub>TD,C</sub> , FF <sub>sIoU,C</sub>	–	[0, 1, 2, 3]	–	$[10^{-3}, 10^{-2}, 10^{-1}, 0.5, 1, 10, 100]$	–

Table 6: Model-specific hyperparameters and their possible values. Models not shown do not have any additional hyperparameters besides those in Table 5.  $L_t$  and  $L_f$  represent the number of transformer layers and fully connected layers, respectively, while  $n_{att}$  represents the number of attention heads,  $\lambda_C$  represents the weight for the cardinality loss, and  $\lambda_{eos}$  represents the weight applied to the end of sequence loss.

Model	Backbone	$L_t$	$L_f$	embedding size	$n_{att}$	$l_r$	$\lambda_C$	$\lambda_{eos}$	scale	dropout rate	weight decay	total # of parameters
TF	ResNet-50	3	–	512	8	$10^{-4}$	–	–	0.1	0.0	$10^{-4}$	32 469 589
TF <sub>shuffle</sub>	ResNet-50	1	–	512	8	$10^{-4}$	–	–	0.1	0.1	$10^{-4}$	27 210 325
TF <sub>set</sub>	ResNet-50	1	–	512	8	$10^{-4}$	–	0.5	0.1	0.1	$10^{-4}$	27 210 325
LSTM	ResNet-50	–	–	2048	–	$10^{-4}$	–	–	0.1	0.5	$10^{-4}$	94 927 958
LSTM <sub>shuffle</sub>	ResNet-50	–	–	2048	–	$10^{-3}$	–	–	$10^{-2}$	0.5	0.0	94 927 958
LSTM <sub>set</sub>	ResNet-50	–	–	1024	–	$10^{-3}$	–	0.1	$10^{-2}$	0.0	$10^{-4}$	43 491 414
FF <sub>BCE</sub>	ResNet-50	–	0	2048	–	$10^{-3}$	–	–	$10^{-2}$	0.5	$10^{-4}$	23 549 012
FF <sub>BCE,C</sub>	ResNet-50	–	1	2048	–	$10^{-4}$	$10^{-2}$	–	0.1	0.3	0.0	27 761 755
FF <sub>BCE,DC</sub>	ResNet-50	–	0	2048	–	$10^{-3}$	–	–	$10^{-2}$	0.3	0.0	23 563 355
FF <sub>sIoU</sub>	ResNet-50	–	2	2048	–	$10^{-4}$	–	–	0.1	0.0	$10^{-4}$	31 945 812
FF <sub>sIoU,C</sub>	ResNet-50	–	2	2048	–	$10^{-4}$	$10^{-2}$	–	0.1	0.1	$10^{-4}$	31 960 155
FF <sub>TD</sub>	ResNet-50	–	3	512	–	$10^{-3}$	–	–	$10^{-2}$	0.0	0.0	25 357 396
FF <sub>TD,C</sub>	ResNet-50	–	3	512	–	$10^{-4}$	0.1	–	0.1	0.0	$10^{-4}$	25 360 987
FF <sub>BCE</sub>	ResNet-101	–	0	2048	–	$10^{-3}$	–	–	$10^{-2}$	0.1	$10^{-4}$	42 541 140
LSTM	ResNet-101	–	–	2048	–	$10^{-3}$	–	–	$10^{-2}$	0.3	$10^{-4}$	113 920 086
FF <sub>BCE</sub>	ResNeXt-101-32x8d	–	2	512	–	$10^{-4}$	–	–	0.1	0.3	0.0	88 328 532
LSTM	ResNeXt-101-32x8d	–	–	1024	–	$10^{-4}$	–	–	$10^{-2}$	0.5	0.0	106 725 718

Table 7: **Hyperparameter values chosen by HYPERBAND for VOC.**  $L_t$  and  $L_f$  represent the number of transformer layers and fully connected layers, respectively, while  $n_{att}$  represents the number of attention heads,  $\lambda_C$  refers to the weight for the cardinality loss,  $l_r$  to the learning rate,  $\lambda_{eos}$  to the weight applied to the end of sequence loss and scale refers to the ratio between the image encoder’s and set predictor’s learning rates.

Model	Backbone	$L_t$	$L_f$	embedding size	$n_{att}$	$l_r$	$\lambda_C$	$\lambda_{eos}$	scale	dropout rate	weight decay	total # of parameters
TF	ResNet-50	2	—	256	2	$10^{-3}$	—	—	$10^{-2}$	0.1	$10^{-4}$	25 394 065
TF <sub>shuffle</sub>	ResNet-50	2	—	512	4	$10^{-4}$	—	—	0.1	0.1	0.0	29 901 457
TF <sub>set</sub>	ResNet-50	3	—	512	2	$10^{-4}$	—	0.5	0.1	0.1	0.0	32 531 089
LSTM	ResNet-50	—	—	1024	—	$10^{-3}$	—	—	$10^{-2}$	0.1	$10^{-4}$	43 614 354
LSTM <sub>shuffle</sub>	ResNet-50	—	—	2048	—	$10^{-4}$	—	—	0.1	0.1	$10^{-4}$	95 173 778
LSTM <sub>set</sub>	ResNet-50	—	—	2048	—	$10^{-4}$	—	0.1	0.1	0.0	0.0	95 173 778
FF <sub>BCE</sub>	ResNet-50	—	2	512	—	$10^{-3}$	—	—	$10^{-2}$	0.1	0.0	25 125 008
FF <sub>BCE,C</sub>	ResNet-50	—	3	2048	—	$10^{-4}$	$10^{-2}$	—	0.1	0.1	0.0	36 306 083
FF <sub>BCE,DC</sub>	ResNet-50	—	2	2048	—	$10^{-3}$	—	—	$10^{-2}$	0.5	0.0	32 107 683
FF <sub>sIoU</sub>	ResNet-50	—	1	2048	—	$10^{-4}$	—	—	$10^{-2}$	0.0	0.0	27 870 352
FF <sub>sIoU,C</sub>	ResNet-50	—	2	2048	—	$10^{-4}$	$10^{-2}$	—	$10^{-2}$	0.0	$10^{-4}$	32 107 683
FF <sub>TD,C</sub>	ResNet-50	—	2	1024	—	$10^{-3}$	0.1	—	$10^{-2}$	0.1	$10^{-4}$	27 809 955
FF <sub>BCE</sub>	ResNet-101	—	1	2048	—	$10^{-4}$	—	—	0.1	0.0	0.0	46 862 480
LSTM	ResNet-101	—	—	512	—	$10^{-3}$	—	—	$10^{-2}$	0.0	$10^{-4}$	48 096 914
FF <sub>BCE</sub>	ResNeXt-101-32x8d	—	2	2048	—	$10^{-4}$	—	—	0.1	0.0	0.0	95 303 056
LSTM	ResNeXt-101-32x8d	—	—	512	—	$10^{-3}$	—	—	$10^{-2}$	0.1	$10^{-4}$	92 339 090

Table 8: **Hyperparameter values chosen by HYPERBAND for COCO.**  $L_t$  and  $L_f$  represent the number of transformer layers and fully connected layers, respectively, while  $n_{att}$  represents the number of attention heads,  $\lambda_C$  refers to the weight for the cardinality loss,  $l_r$  to the learning rate,  $\lambda_{eos}$  to the weight applied to the end of sequence loss and scale refers to the ratio between the image encoder’s and set predictor’s learning rates.

Model	Backbone	$L_t$	$L_f$	embedding size	$n_{att}$	$l_r$	$\lambda_C$	$\lambda_{eos}$	scale	dropout rate	weight decay	total # of parameters
TF	ResNet-50	3	—	256	4	$10^{-4}$	—	—	0.1	0.0	$10^{-4}$	26 054 034
TF <sub>shuffle</sub>	ResNet-50	1	—	512	8	$10^{-4}$	—	—	$10^{-2}$	0.3	0.0	27 272 850
TF <sub>set</sub>	ResNet-50	1	—	256	4	$10^{-4}$	—	0.1	0.1	0.1	0.0	24 735 122
LSTM	ResNet-50	—	—	2048	—	$10^{-4}$	—	—	$10^{-2}$	0.3	$10^{-4}$	95 177 875
LSTM <sub>shuffle</sub>	ResNet-50	—	—	256	—	$10^{-4}$	—	—	0.1	0.5	0.0	25 192 851
LSTM <sub>set</sub>	ResNet-50	—	—	1024	—	$10^{-4}$	—	0.1	$10^{-2}$	0.3	0.0	43 616 403
FF <sub>BCE</sub>	ResNet-50	—	1	2048	—	$10^{-4}$	—	—	0.1	0.1	0.0	27 872 401
FF <sub>BCE,C</sub>	ResNet-50	—	1	1024	—	$10^{-4}$	$10^{-2}$	—	0.1	0.1	0.0	26 754 206
FF <sub>BCE,DC</sub>	ResNet-50	—	1	1024	—	$10^{-3}$	—	—	$10^{-2}$	0.3	0.0	26 754 206
FF <sub>sIoU</sub>	ResNet-50	—	1	2048	—	$10^{-4}$	—	—	0.1	0.1	0.0	27 872 401
FF <sub>sIoU,C</sub>	ResNet-50	—	1	1024	—	$10^{-4}$	$10^{-2}$	—	0.1	0.0	0.0	26 754 206
FF <sub>TD,C</sub>	ResNet-50	—	2	2048	—	$10^{-4}$	0.5	—	0.1	0.0	$10^{-4}$	32 097 438
FF <sub>BCE</sub>	ResNet-101	—	1	2048	—	$10^{-4}$	—	—	$10^{-2}$	0.3	0.0	46 864 529
LSTM	ResNet-101	—	—	2048	—	$10^{-4}$	—	—	$10^{-2}$	0.0	$10^{-4}$	114 170 003
FF <sub>BCE</sub>	ResNeXt-101-32x8d	—	1	2048	—	$10^{-4}$	—	—	$10^{-2}$	0.3	0.0	91 106 705
LSTM	ResNeXt-101-32x8d	—	—	1024	—	$10^{-4}$	—	—	$10^{-2}$	0.0	0.0	106 850 707

Table 9: **Hyperparameter values chosen by HYPERBAND for NUS-WIDE.**  $L_t$  and  $L_f$  represent the number of transformer layers and fully connected layers, respectively, while  $n_{att}$  represents the number of attention heads,  $\lambda_C$  refers to the weight for the cardinality loss,  $l_r$  to the learning rate,  $\lambda_{eos}$  to the weight applied to the end of sequence loss and scale refers to the ratio between the image encoder’s and set predictor’s learning rates.

Model	Backbone	$L_t$	$L_f$	embedding size	$n_{att}$	$l_r$	$\lambda_C$	$\lambda_{eos}$	scale	dropout rate	weight decay	total # of parameters
TF	ResNet-50	1	–	256	4	$10^{-3}$	–	–	0.1	0.1	$10^{-4}$	24 770 519
TF <sub>shuffle</sub>	ResNet-50	2	–	256	8	$10^{-3}$	–	–	0.1	0.1	0.0	25 429 975
TF <sub>set</sub>	ResNet-50	2	–	1024	8	$10^{-4}$	–	0.1	0.1	0.1	$10^{-4}$	46 923 991
LSTM	ResNet-50	–	–	2048	–	$10^{-3}$	–	–	$10^{-2}$	0.3	$10^{-4}$	95 460 568
LSTM <sub>shuffle</sub>	ResNet-50	–	–	512	–	$10^{-3}$	–	–	0.1	0.0	0.0	29 176 536
LSTM <sub>set</sub>	ResNet-50	–	–	1024	–	$10^{-3}$	–	0.1	0.1	0.0	0.0	43 757 784
FF <sub>BCE</sub>	ResNet-50	–	0	1024	–	$10^{-2}$	–	–	$10^{-2}$	0.1	0.0	25 760 982
FF <sub>BCE,C</sub>	ResNet-50	–	0	2048	–	$10^{-3}$	$10^{-2}$	–	$10^{-2}$	0.1	$10^{-4}$	23 878 901
FF <sub>BCE,DC</sub>	ResNet-50	–	3	2048	–	$10^{-4}$	–	–	0.1	0.1	0.0	36 474 101
FF <sub>sIoU</sub>	ResNet-50	–	1	2048	–	$10^{-4}$	–	–	0.1	0.0	0.0	28 013 782
FF <sub>sIoU,C</sub>	ResNet-50	–	1	2048	–	$10^{-4}$	$10^{-3}$	–	0.1	0.0	0.0	28 077 301
FF <sub>TD</sub>	ResNet-50	–	1	2048	–	$10^{-2}$	–	–	$10^{-2}$	0.1	0.0	28 013 782
FF <sub>TD,C</sub>	ResNet-50	–	2	2048	–	$10^{-3}$	$10^{-2}$	–	0.1	0.1	0.0	32 275 701
FF <sub>BCE</sub>	ResNet-101	–	1	2048	–	$10^{-4}$	–	–	0.1	0.0	0.0	47 005 910
LSTM	ResNet-101	–	–	512	–	$10^{-3}$	–	–	$10^{-2}$	0.0	$10^{-4}$	48 168 664
FF <sub>BCE</sub>	ResNeXt-101-32x8d	–	0	2048	–	$10^{-3}$	–	–	$10^{-2}$	0.0	$10^{-4}$	87 049 686
LSTM	ResNeXt-101-32x8d	–	–	256	–	$10^{-3}$	–	–	$10^{-2}$	0.1	$10^{-4}$	88 462 552

Table 10: **Hyperparameter values chosen by HYPERBAND for ADE20k.**  $L_t$  and  $L_f$  represent the number of transformer layers and fully connected layers, respectively, while  $n_{att}$  represents the number of attention heads,  $\lambda_C$  refers to the weight for the cardinality loss,  $l_r$  to the learning rate,  $\lambda_{eos}$  to the weight applied to the end of sequence loss and scale refers to the ratio between the image encoder’s and set predictor’s learning rates.

Model	Backbone	$L_t$	$L_f$	embedding size	$n_{att}$	$l_r$	$\lambda_C$	$\lambda_{eos}$	scale	dropout rate	weight decay	total # of parameters
TF	ResNet-50	1	–	2048	8	$10^{-4}$	–	–	0.1	0.3	$10^{-4}$	71 582 223
TF <sub>shuffle</sub>	ResNet-50	2	–	256	4	$10^{-3}$	–	–	0.1	0.1	0.0	26 115 343
TF <sub>set</sub>	ResNet-50	2	–	256	2	$10^{-3}$	–	$10^{-3}$	0.1	0.1	0.0	26 115 343
LSTM	ResNet-50	–	–	2048	–	$10^{-4}$	–	–	0.1	0.5	$10^{-4}$	100 934 160
LSTM <sub>shuffle</sub>	ResNet-50	–	–	2048	–	$10^{-3}$	–	–	0.1	0.1	$10^{-4}$	100 934 160
LSTM <sub>set</sub>	ResNet-50	–	–	2048	–	$10^{-4}$	–	$10^{-3}$	0.1	0.5	0.0	100 934 160
FF <sub>BCE</sub>	ResNet-50	–	2	2048	–	$10^{-3}$	–	–	$10^{-2}$	0.0	0.0	34 949 646
FF <sub>BCE,C</sub>	ResNet-50	–	3	2048	–	$10^{-3}$	$10^{-3}$	–	$10^{-2}$	0.1	0.0	39 189 026
FF <sub>BCE,DC</sub>	ResNet-50	–	2	1024	–	$10^{-3}$	–	–	$10^{-2}$	0.3	0.0	29 252 130
FF <sub>sIoU</sub>	ResNet-50	–	1	2048	–	$10^{-4}$	–	–	0.1	0.1	0.0	30 751 246
FF <sub>sIoU,C</sub>	ResNet-50	–	1	1024	–	$10^{-3}$	0.1	–	$10^{-2}$	0.0	0.0	28 201 506
FF <sub>TD</sub>	ResNet-50	–	3	1024	–	$10^{-4}$	–	–	0.1	0.0	$10^{-4}$	30 282 254
FF <sub>TD,C</sub>	ResNet-50	–	2	2048	–	$10^{-3}$	$10^{-3}$	–	0.1	0.0	0.0	34 990 626
FF <sub>BCE</sub>	ResNet-101	–	0	512	–	$10^{-3}$	–	–	0.1	0.3	0.0	44 312 078
LSTM	ResNet-101	–	–	2048	–	$10^{-4}$	–	–	0.1	0.5	$10^{-4}$	119 926 288
FF <sub>BCE</sub>	ResNeXt-101-32x8d	–	3	2048	–	$10^{-4}$	–	–	0.1	0.0	0.0	102 382 350
LSTM	ResNeXt-101-32x8d	–	–	1024	–	$10^{-4}$	–	–	0.1	0.1	$10^{-4}$	109 729 552

Table 11: **Hyperparameter values chosen by HYPERBAND for Recipe1M.**  $L_t$  and  $L_f$  represent the number of transformer layers and fully connected layers, respectively, while  $n_{att}$  represents the number of attention heads,  $\lambda_C$  refers to the weight for the cardinality loss,  $l_r$  to the learning rate,  $\lambda_{eos}$  to the weight applied to the end of sequence loss and scale refers to the ratio between the image encoder’s and set predictor’s learning rates.